Collaborative Optimization of Multi-regional Integrated Energy System Based on Improved Beluga Whale Optimization Algorithm

Ming Liu

School of Control and Computer Engineering, North China Electric Power University, Beijing 102206, China
E-mail: 2276899015@qq.com

Received 19 April 2024; Accepted 20 May 2024

Abstract

With the installed capacity of the renewable energy power generation is growing at a high speed, a large number of the renewable energy is connected to the grid, the energy problem has been solved to a large extent, but the ensuing problems can not be ignored, the first is the consumption of the renewable energy, which is followed by the stability problem of the power system, and a multi-regional integrated energy system (MRIES) is constructed to solve the problem. In view of the wind power uncertainty, the absorption treatment is carried out by the equipment layer and the optimization layer respectively. A hybrid energy storage system (HESS) is introduced in the equipment layer to suppress the influence of the wind power uncertainty on the system stability. A combination of the convolutional filtering algorithm, the Improved Complete Ensemble Empirical Mode Decomposition with Adaptive Noise algorithm and the fuzzy control algorithm is introduced in the optimization layer to develop the charging and discharging strategy of the HESS. With the strategy, the impact of the electric power fluctuations on the power system during the optimization process can be reduced largely. Then, on the basis of fully considering the energy coupling in different equipments, a collaborative

Distributed Generation & Alternative Energy Journal, Vol. 39_4, 717–750.
doi: 10.13052/dgaej2156-3306.3942

optimization model of the MRIES is constructed. And the integrated demand response model considering the time-of-use electric price is introduced in the load side. Finally, the improved Beluga optimization(IBWO) algorithm is developed to optimize the model. The optimization results show that the IBWO algorithm plays a good optimization effect both in the participation of energy supply equipments and the economy, plays a collaborative optimization role in the MRIES and ensures the stability of the whole power system.

Keywords: Multi-regional integrated energy system, wind power uncertainty, hybrid energy storage, collaborative optimization, improved beluga whale optimization algorithm.

1 Introduction

In today's situation of the rapid development, the energy shortage problem and the renewable energy consumption problem has become more important that needs to be solved in our country, and the integrated energy system (IES), as a research hotspot of the domestic and foreign experts, has become the key to solve energy problems [1]. Since the output of the renewable energy is random and intermittent, we must pretreat it firstly, and only in this way can the stability of the IES be guaranteed [2]. Considering the spatial correlation of the wind power uncertainty, an adaptive robust collaborative optimization method for energy reserve was developed [3]. The study in Ref. [4] used the chance constraints to cope with the wind power uncertainty. And a method that described the multiple uncertainties of the wind power was proposed in Ref. [5].

Of course, in addition to ensuring the stability of the energy output power, we should also regulate the user's energy on the load side as much as possible, so as to avoid the imbalance. The study in Ref. [6] analyzed the typical seasonal multi-energy load curve of various functional zones in a comprehensive energy system in North China, fully explored the independent energy demand and energy use characteristics of each region in the system and the complementary relationship between regions, and designed differentiated multi-energy equipment planning alternatives in different regions, so as to reduce the scale of the multi-regional collaborative planning effectively. And a demand response model concluding the incentive price and the demand response coefficient was proposed in Ref. [7]. The study in Ref. [8] proposed a new unified spatio-temporal cooperative scheduling framework for

trans-regional IESs, which could cope with the renewable energy uncertainty. And a risk assessment method of the IES planning scheme considering the conditional risk value was developed [9].

With the study of the source-load uncertainty, more and more studies begin to consider source-load uncertainty comprehensively [10]. To describe the probability distribution of the wind output power accurately, the scenario analysis method in stochastic optimization was developed to cope with the uncertainty of the load at first, and then the two-stage robust optimization method was developed to deal with the uncertainty of the price-type demand-side response to realize the cooperative scheduling of the source, the load and the storage [11]. And a nonlinear interval number method was used to characterize the source-load uncertainty effectively in Ref. [12]. In order to coordinate the flexible demand response and the multiple renewable energy generation uncertainty, a double-layer model for a community IES was proposed in a multi-stakeholder scenario [13]. And a hybrid robust interval optimization method was developed for the IES planning with uncertainties in Ref. [14]. Aiming at the uncertainties of multi-operator behaviors in a regional IES, the fuzzy parameters were introduced to estimate the source-load uncertainty considering the fuzzy opportunity constraint programming [15]. To solve the renewable distributed energy generation uncertainty effectively, opportunity constraints were used and a quantile prediction method was developed based on the gradient enhanced regression tree [16]. Considering the load forecasting uncertainty, a multi-objective stochastic optimization method was proposed based on multiple uncertainties [17].

Besides, there were some literatures to study the correlation between the source uncertainty and the load uncertainty. In Ref. [18], by using the scene tree structure, 32 probabilistic random scenarios were generated to simulate the correlation and uncertainty among photovoltaic generator sets, wind turbines and multiple energy loads. And the study in Ref. [19] proposed a method that considerd the uncertainty relationships between the source and the load, besides, the Wasserstein deep convolution generation was used to capture the correlation between uncertainties.

It is the so-called collaborative optimization of the multi-regional integrated energy system(MRIES) that carries out the power distribution of the load for multiple systems and multiple energy equipments to achieve a good control effect. The study in Ref. [20] proposed an improved multi-agent depth deterministic strategy gradient method, which used the centralized training and the decentralized execution framework to improve the stability of the

MRIES effectively. A cooperative optimization strategy of the regional IES was developed based on the multi-agent consistency, which could cope with the uncertain effects of various energy generation and demand flexiblies [21]. In order to improve the operation flexibility of the IES, a collaborative operation optimization strategy of the IES was developed [22]. And a multi-agent operation strategy was proposed in Ref. [23], including energy retailers, suppliers and users. The study in Ref. [24] introduced a low-carbon operation strategy of the MRIES based on the mixed game theory, and established an interactive mechanism of the multi-agent low-carbon economy operation. The cascaded storage system and multi-time scale operation strategy were developed to promote the coordinated control capability of the IESs [25]. The study in Ref. [26] proposed an operation optimization strategy based on the non-dominated sorting genetic algorithm to achieve the efficient energy utilization better. And a multi-time scale coordinated control strategy was adopted in Ref. [27], it can be well coupled with the system, and solve the problem effectively that the cold cogeneration equipments, energy storage equipments and power storage equipments need to operate under different time scales. The study in Ref. [28] designed a differential evolution algorithm based on the reinforcement learning, so that the optimal mutation strategy and the related parameters could be determined adaptively. And a two-layer cooperative optimization method consisting of upper optimization configuration and lower optimization operation was proposed in Ref. [29]. Besides, a multi-layer control strategy based on component response state partitioning system was proposed in Ref. [30]. The study in Ref. [31] developed an adaptive adjustment strategy considering the time characteristics, which greatly improved the optimization reliability and the ability to manage the wind power uncertainty in the IES. The study in Ref. [32] adopted a multi-scale optimization strategy based on the the source and the load forecasting, which improved the energy utilization rate of the regional IES significantly. The study in Ref. [33] proposed a multi-time scale optimization operation strategy of the IES considering the demand response mechanism. And a Stackelberg dynamic price strategy was established in Ref. [34] in which the IES is the upper leader, the mixed charging station is the lower follower, and the electricity price is the sole interactive information. The study in Ref. [35] introduced a unified spatio-temporal cooperation framework for the IESs, in which the coordination of the multi-energy coupling and the multi-agent system energy sharing took into account. The study in Ref. [36] developed a new two-layer stochastic optimization framework considering multiple scenarios to optimize the IES capacity and operation. A carbon capture device operation

strategy based on the stepped carbon penalty response was proposed, which solved the economic problem of the carbon capture in the IES [37]. The study in Ref. [38] established a distributed multi-agent collaborative optimization model, and adopted the alternating direction multiplier algorithm to solve its two sub-problems, thus protecting the privacy of each agent effectively. And the study in Ref. [39] proposed an improved action selection strategy to enhance the local optimization by introducing the "offset" according to the probability in the training process.

This paper constructs a MRIES including electricity, gas, cold, thermal and storage. Firstly, different devices are classified according to their energy coupling characteristics, and then the different energy subsystems are modularized according to their classifications. Secondly, in view of the wind power uncertainty, a new approach is carried out both in the equipment layer and the optimization layer respectively. In the equipment layer, the hybrid energy storage system (HESS) is introduced to suppress the influence of the wind power uncertainty on the system stability. In the optimization layer, the convolutional filtering algorithm, the Improved Complete Ensemble Empirical Mode Decomposition with Adaptive Noise (ICEEMDAN) algorithm and the fuzzy control algorithm are combined to formulate the charging and discharging strategy of the HESS. Finally, under the circumstance of fully considering the energy coupling in different devices, a collaborative optimization model of the MRIES is constructed. On the load side, a integrated demand response model considering the time-of-use (TOU) electricity price mechanism is introduced. At last, the Improved Beluga Whale Optimization (IBWO) algorithm is adopted to optimize the model. Compared with the Beluga Whale Optimization (BWO) algorithm, the improved strategies is as follows:

(1) The Tent chaotic mapping strategy is adopted to improve the quality of the initial solution of the population.
(2) The adaptive T-distribution mutation strategy is adopted to improve population diversity and optimization ability.
(3) The Gaussian walk strategy is adopted to further improve the global search ability of the algorithm and avoid the algorithm falling into the local optimal solution.

The structure of this paper is as follows: Section 2 constructs the MRIES model including the electric system, the thermal system, and the cold system, makes constraints on the different energy power of the MRIES and introduces a integrated demand response model. Section 3 proposes a hybrid energy

storage solution strategy to solve the wind power uncertainty. Section 4 studies a collaborative optimization strategy based on the MRIES and uses the IBWO algorithm to coordinate it, Section 5 are the results and discussion and the Section 6 is the conclusion.

2 Model of the MRIES

As the most important energy system and structure in the future energy field, the modular and fine modeling of the electric-thermal-cold IES is the basis for realizing the energy utilization, the energy saving and the emission reduction. And all of the energy supply equipments are modeled from three aspects: electricity, thermal and cold. And a comprehensive model of the electric-thermal-cold energy system will be built by fully reflecting its characteristics.

In this chapter, in addition to the five kinds of electric load power supply devices including the wind turbines, the photovoltaic cells, the fuel cells, the gas turbines and the ORC waste thermal generation devices, three kinds of thermal load power supply devices including the thermal pumps, the gas boilers and the gas turbines, and two kinds of cold load power supply devices including the absorption refrigerators and the electric refrigerators are modeled, various power constraints of the whole MRIES, including the electric power, the thermal power, the cold power, the energy networks interaction power and the grid interaction power, are modeled as well. Finally, an integrated demand response model based on the TOU electricity price mechanism is established. The load power supply structure of the IES in each region is shown in Figure 1:

2.1 Electric System Model

2.1.1 Wind turbine model

The wind turbine work by capturing kinetic energy in the air through the blades and converting mechanical energy into electricity through the wind turbine. When the wind wheel coefficient, blade area and air density are unchanged, the fan output power is only related to the wind speed. The simplified mathematical model is as follow:

$$P_{wt}(v) = \begin{cases} 0, & 0 \le v < v_{ci} \\ P_r \dfrac{v^2 - v_{ci}^2}{v_r^2 - v_{ci}^2}, & v_{ci} \le v \le v_r \\ P_r, & v_r < v \le v_{co} \\ 0, & v_{co} < v \end{cases} \tag{1}$$

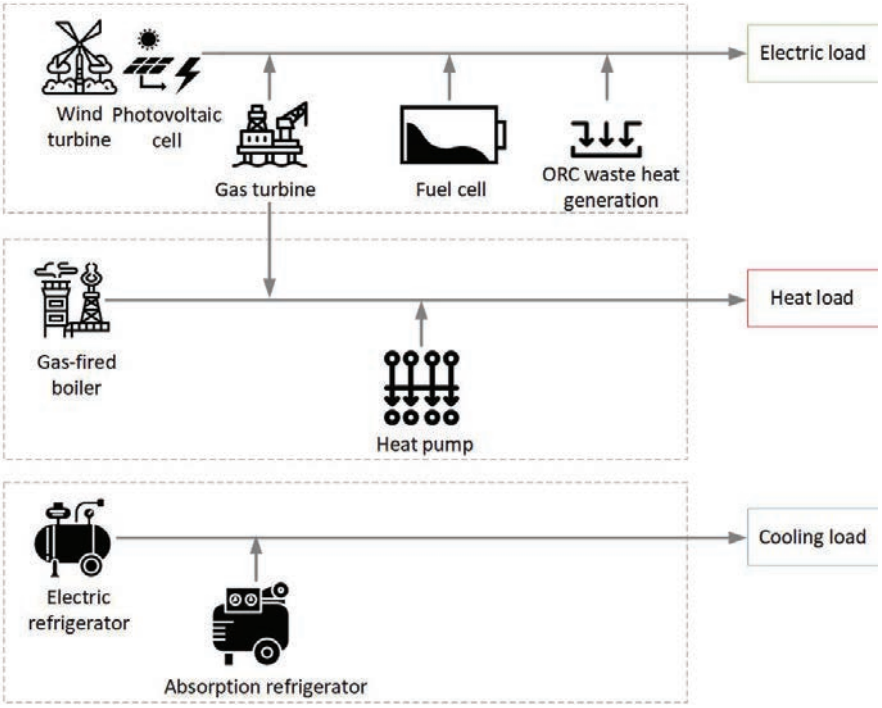

Figure 1 Load power supply structure diagram of IES in each region.

In formula (1): v represents the wind speed at the height of air blower hub, v_{ci}, v_{co}, v_r represent the cut in, cut out and rated wind speed respectively, and P_r represents the rated power. And in this paper, the value of v_{ci}, v_{co}, v_r is 3, 15, and 6, in m/s. The P_r value is 1500, in MW.

The power constraint of the wind turbine is as follow:

$$\underline{P}_{wt} \leq P_{wt}(v) \leq \overline{P}_{wt} \tag{2}$$

In formula (2), $\underline{P}_{wt}$, $\overline{P}_{wt}$ represent the upper and lower power limit of the wind turbine respectively.

2.1.2 Photovoltaic cell model

The power of the photovoltaic cell is affected by the temperature of the photovoltaic panels and the light intensity, the output power formula of photovoltaic panels is as follow:

$$P_{st} = A_{st} R_{st} \eta_{st} \tag{3}$$

In formula (3), A_{st} represents the area of the photovoltaic power generation panel, which is 25000 in this paper, η_{st} represents the power generation efficiency coefficient of the photovoltaic cell, and the value in this paper is 0.16, R_{st} represents the light intensity of the photovoltaic power generation panels at different times, it can be obtained by the following formula:

$$R_{st} = R/1000 \tag{4}$$

In formula (4), R represents the actual light intensity at different times.

The power constraint of the photovoltaic cell is as follow:

$$\underline{P}_{st} \leq P_{st} \leq \overline{P}_{st} \tag{5}$$

In formula (5), $\underline{P}_{st}$, $\overline{P}_{st}$ represent the upper and lower power limits of the photovoltaic cell respectively.

2.1.3 Fuel cell model

The fuel cell consumes hydrogen to produce electricity, and the power expression is:

$$P_t^{FC} = \alpha \cdot V_{H_2}^{FC} \tag{6}$$

In formula (6), P_t^{FC}, $V_{H_2}^{FC}$ represent the electric output power and the hydrogen volume respectively, and α is the energy conversion coefficient.

The power constraint of the fuel cell is as follow:

$$0 \leq P_t^{FC} \leq 3500 \tag{7}$$

2.1.4 Gas turbine model

In addition to meeting the electric energy demand, the gas turbine need to serve as an auxiliary energy source to meet the thermal energy demand. The mathematical model is shown as follow:

$$P_t^{GT} = V_t^{GT} \eta^{GT} \beta / \Delta t \tag{8}$$

$$H_t^{HRB} = P_t^{GT} \eta^{HRB} (1 - \eta^{GT}) / \eta^{GT} \tag{9}$$

In formula (8) and (9), P_t^{GT} represents the electric output power, V_t^{GT} represents the gas consumption, and η^{GT} represents power generation efficiency, which is 0.3 in this paper, β represents the calorific value of the natural gas, which is 9.97 kWh/m^3 in this paper. H_t^{HRB} represents the thermal output power of the waste thermal boiler, and η^{HRB} represents the waste thermal recovery efficiency, the value in this paper is 0.8.

The power constraint of the gas turbine is as follow:

$$0 \leq P_t^{GT} \leq 5500 \tag{10}$$

2.1.5 ORC waste thermal power generation device model

Compared with the conventional steam Rankine cycle, the ORC waste thermal power generation device has a higher efficiency in recovering the waste thermal, which can be converted into more electrical energy. The power expression is as follow:

$$P_t^{ORC} = H_t^{ORC} \eta^{ORC} \tag{11}$$

In formula (11), P_t^{ORC} and H_t^{ORC} represent the electrical output power and thermal output power of the ORC waste thermal power generation device respectively, η^{ORC} is the thermal-electric energy conversion coefficient, which is 0.18 in this paper.

The power constraint of the ORC waste thermal power generation device is as follow:

$$0 \leq P_t^{ORC} \leq 1200 \tag{12}$$

2.2 Thermal System Model

2.2.1 Thermal pump model

In this paper, the air source thermal pump is selected as a comprehensive energy system thermal pump device, and the air is used as the thermal source of the thermal pump, which has multiple advantages: inexhaustible, unlimited and free access. In addition, the air source thermal pump is more convenient in both the installation and the use. The working characteristic of the air source thermal pump device is as follow:

$$H_t^{EHP} = P_t^{EHP} \lambda_{COP} \tag{13}$$

In formula (13), H_t^{EHP} and P_t^{EHP} represent the thermal output power and the electric input power of the thermal pump device respectively, and λ_{COP} is the electric-thermal energy conversion coefficient of the thermal pump device, which is 2.5 in this paper.

The value of the thermal pump is that when the IES has superfluous renewable energy power, the gas turbine power can be reduced, and the thermal pump device is used to compensate for the partial reduction, while consuming part of the electric energy. By using a thermal pump device to change the ratio of electrical load and thermal load, the problem of wind

curtailment in the IES is solved, and the purpose of reducing the energy storage devices' repeated charging and discharging behaviors and saving the natural gas consumption is also achieved.

The power constraint of the thermal pump is as follow:

$$0 \leq H_t^{EHP} \leq 3500 \tag{14}$$

2.2.2 Gas-fired boiler model

The gas-fired boiler obtains the hot water or the high-temperature water vapor by burning natural gas, which provides part of the thermal energy. Under normal operating conditions, the thermal efficiency is very stable and can reach the 90% above. Its mathematical expression is as follow:

$$H_t^{\mathrm{GB}} = V_t^{\mathrm{GB}} \eta^{\mathrm{GB}} \beta / \Delta t \tag{15}$$

In formula (15), H_t^{GB} represents the thermal output power of the gas boiler, V_t^{GB} represents the intake air value, η^{GB} represents the thermal efficiency under normal operating conditions, and the value in this paper is 0.8, β represents the calorific value of the natural gas.

The power constraint is as follow:

$$0 \leq H_t^{GB} \leq 4000 \tag{16}$$

2.3 Cold System Model

2.3.1 Absorption refrigerator model

In this paper, the lithium bromide absorption refrigerating machine is used as the absorption refrigeration equipment, it can convert the thermal energy into cold power, and the thermal-cold conversion efficiency is generally between (1,2). The mathematical model is shown as follow:

$$C_t^{LB} = H_t^{LB} COP_{LB} \tag{17}$$

In formula (17), C_t^{LB} represents the cold output power of the absorption refrigerator, H_t^{LB} represents the thermal input power, and COP_{LB} refers to the thermal-cold conversion coefficient, which is 1.5 in this paper.

The power constraint of the absorption refrigerator is as follow:

$$0 \leq C_t^{LB} \leq 3500 \tag{18}$$

2.3.2 Electric refrigeration unit model

In this paper, the same type of electric chillers are used in the electric refrigeration unit, the mathematical model is shown as follow:

$$\begin{cases} C_t^{EC} = \eta_{ec} P_t^{EC} \\ P_{\min}^{EC} \leq P_t^{EC} \leq P_{\max}^{EC} \end{cases} \tag{19}$$

In formula (19), P_t^{EC} represents the electric input power of the electric refrigerator unit, C_t^{EC} represents the cold output power, η_{ec} is the electric-cold energy conversion coefficient, which is 2.8 in this paper, and $P_{\min}^{EC}$ and $P_{\max}^{EC}$ represent the minimum value and the maximum value of the electric power respectively.

The power constraint of the electric refrigeration unit is as follow:

$$0 \leq C_t^{EC} \leq 2200 \tag{20}$$

2.4 Power Constraints of MRIES

2.4.1 Electrical power constraints

The IES of each region carries out the load supply through five parts mainly: wind power, photovoltaic power, fuel cell power, gas turbine power and ORC waste thermal generation power, and at the same time the thermal pump devices and the electric refrigeration units consume the electric power. The electrical power constraints are as follows:

$$\begin{aligned} E_{\text{load}} = {} & P_t^{GT} + P_t^{FC} + P_t^{ORC} + P_{wt} + P_{st} + P_{grid} \\ & + P_{mult} - P_t^{EC} - P_t^{EHP} \end{aligned} \tag{21}$$

$$P_t^{EC} = C_t^{EC} / \eta^{EC} \tag{22}$$

$$P_t^{EHP} = H_t^{EHP} / \lambda_{COP} \tag{23}$$

Formula (21) represents the power balance constraint, E_{load} represents the electrical load demand, P_t^{GT} represents the gas turbine electric power, and P_t^{FC} represents the fuel cell electric power, P_t^{ORC} represents the ORC waste thermal power generation device electric power, P_{wt} represents the wind power, P_{st} represents the photovoltaic power, P_{grid} represents the grid

interaction power between each regional IES and the power grid, and in this paper, it represents the power which is purchased by each regional IES from the power grid, P_{mult} represents the interactive power, P_t^{EC} represents the electric input power of the electric refrigeration unit, P_t^{EHP} represents the thermal pump power, C_t^{EC} represents the refrigeration power of the electric refrigeration unit, η^{EC} represents the electric-cold energy conversion efficiency of the electric refrigeration unit, H_t^{EHP} represents the thermal output power of the thermal pump and λ_{COP} represents the electric-thermal energy conversion efficiency of the thermal pump device.

2.4.2 Thermal power constraints

In the IES of each region, the thermal load in each region is mainly supplied through three parts: the thermal pump power, the gas boiler power and the gas turbine power, meanwhile, the ORC waste thermal power generation devices and absorption chillers consume the thermal power. The thermal power constraints are as follows:

$$H_{load} = H_t^{HRB} + H_t^{EHP} + H_t^{GB} - H_t^{ORC} - H_t^{LB} \tag{24}$$

$$H_t^{HRB} = P_t^{GT}\eta^{HRB}(1-\eta^{GT})/\eta^{GT} \tag{25}$$

$$H_t^{ORC} = P_t^{ORC}/\eta^{ORC} \tag{26}$$

Formula (24) represents the thermal power balance constraint, H_{load} represents the thermal load demand, H_t^{HRB} represents the waste thermal boiler power in the gas boiler, H_t^{EHP} represents the thermal pump power, H_t^{GB} represents the gas boiler power, H_t^{ORC} represents the thermal consumption power of the ORC waste thermal generation, and H_t^{LB} represents the absorption refrigerator power. P_t^{GT} denotes the electric power of the gas turbine, η^{HRB} denotes the recovery efficiency of the waste thermal boiler, and η^{GT} denotes the generation efficiency, H_t^{ORC} and P_t^{ORC} represents the thermal consumption power and the generation power of the ORC waste thermal power generation device respectively.

2.4.3 Cold power constraint

In the IES of each region, the cold load in each region is mainly supplied by two parts: the absorption refrigerator and the electric refrigerator. The cold power constraint is as follow:

$$C_{load} = C_t^{LB} + C_t^{EC} \tag{27}$$

Formula (27) represents the cold power balance constraint, C_t^{LB} represents the absorption refrigerator power, and C_t^{EC} represents the electric refrigerator unit power.

2.4.4 Constraint on the energy grid interactive power

In addition to the energy interaction between the equipments in each regional IES, the energy interaction between the energy networks in each regional IES also exists. Due to the different characteristics of each energy source, this paper considers the electricity interaction between the energy networks, and the constraint of the energy network interactive power is as follow:

$$-5000 \leq P_{mult} \leq 2000 \tag{28}$$

Formula (28) represents the energy networks interaction power constraints of the IES in each region, P_{mult} represents the electricity interaction power between energy networks.

2.4.5 Constraint on the interactive power of the power grid

In addition to the energy interaction between the equipments in each regional IES and the energy interaction between each regional IES, when the renewable energy surplus or the power load is too large, the entire MRIES has excess or insufficient power, the entire MRIES requires to interact with the power grid, supplying power to the power grid or purchasing power from the power grid, the constraint on the interactive power of the power grid is as follow:

$$-5000 \leq P_{grid} \leq 2000 \tag{29}$$

Formula (29) represents the electric power interaction constraint, P_{grid} represents the interactive power between the entire MRIES and the power grid.

2.5 Integrated Demand Response Model

The load of different energy systems has its own unique characteristics. According to the different characteristics of the load, we can formulate the corresponding demand response mechanism. There are three kinds of the energy loads in the IES of each region. Since the thermal load and the cold load are not easy to transmit and save, we have developed the TOU electricity price mechanism according to the energy characteristics of the electricity load and the historical load data, we have developed the corresponding

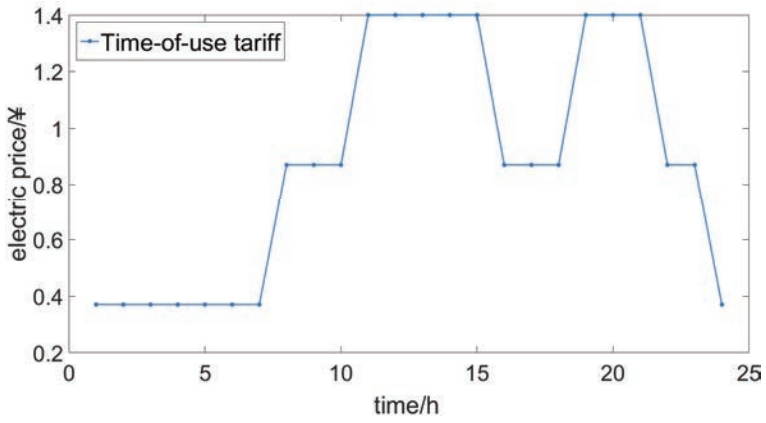

Figure 2 TOU electricity price.

TOU electricity price mechanism. Through the integrated demand response mechanism, we can promote the users to change their reducible load demand. The reducible load refers to a class of the loads that are more sensitive to the changes of the electricity price. When the electricity price changes, the user's reducible load demand will change greatly. When the electricity price become high, the demand of the load will be greatly reduced, so it is called the reducible load. The TOU electricity price in the integrated demand response is shown in Figure 2:

3 Hybrid Energy Storage Solution Strategy

The wind power data which is used in this paper is from the IES simulation platform of Tsinghua University, and the data comes from the typical day of a large wind farm in a southwest region in 2023, and the typical days are 70 days. Therefore, it is taken as a data reference to carry out the simulation experiment in this section. The simulation results are shown below.

First, the convolutional filtering algorithm is used to smooth the wind power data, the difference value between the wind power data before and after smoothing is the upper power limit that the HESS needs to undertake, we takes region three as the example and its specific results are shown in Figures 3 and 4 below:

As shown in Figure 3 above, the wind power data after smoothing is more stable than that before smoothing, so that the wind power will not destroy the stability of the system when it is connected to the IES. By making a difference

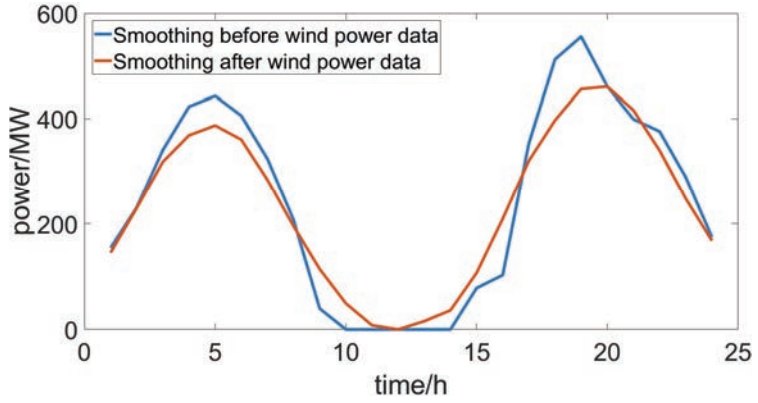

Figure 3 Region three wind power data smoothing before and after comparison.

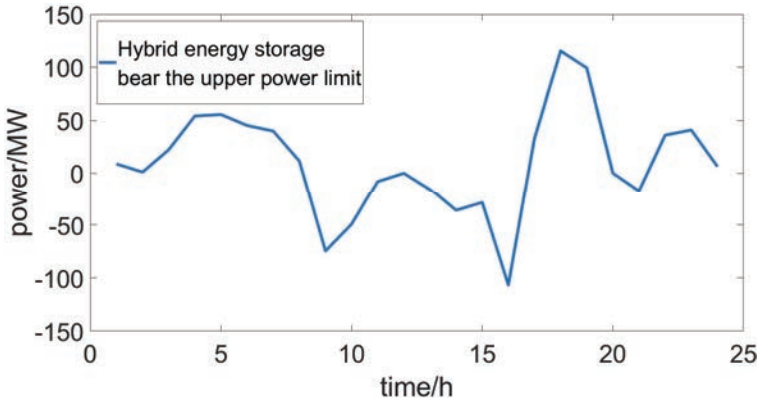

Figure 4 Region three upper power limit diagram of the HESS.

between the wind power data before and after smoothing, the power which the HESS need to undertake can be obtained in Figure 4 above.

3.1 Power Distribution of the HESS

The power which the HESS need to undertake, is taken as the input data of the ICEEMDAN algorithm in this section. First, the Empirical Mode Decomposition method is used to decompose the original signal of the power which the HESS need to undertake into multiple Intrinsic Mode Functions (IMF), and then the noise in each IMF is removed by the adaptive noise algorithm. Finally, the de-noised IMF is integrated fully, and then the decomposed signal is obtained. The specific results are shown in Figures 5 and 6 below:

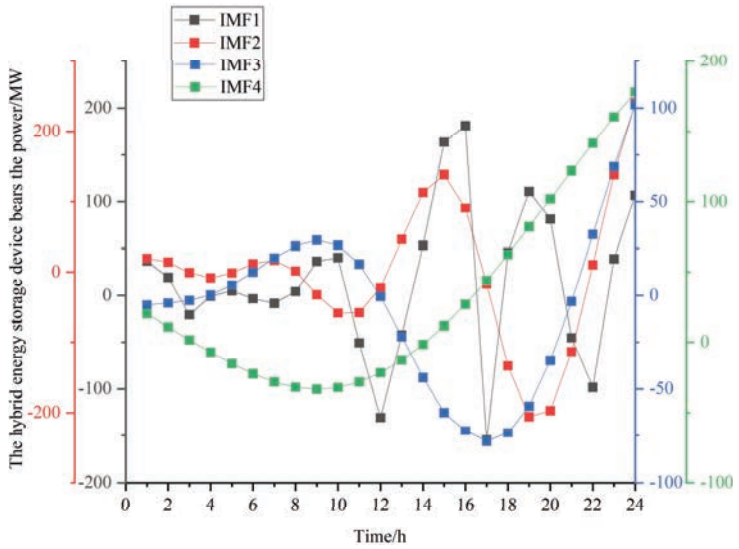

Figure 5 The power decomposition signal assumed by the hybrid energy storage devices.

As shown in Figure 5, the signals of the HESS after power decomposition can be divided into four kinds according to their frequencies, which are IMF1, IMF2, IMF3 and IMF4 respectively from low to high. And then the signals of the different frequencies are allocated to different energy storage devices according to their characteristics. In order to make the power of different frequency bands corresponding to these signals be distributed to the two energy storage devices reasonably in the HESS, namely the lithium battery and the supercapacitor. The four signals are shown in Figure 6 respectively, and the above decomposed data is divided into two kinds of the frequency components, in which the high one is borne by the supercapacitor and the low one is borne by the lithium battery. With the frequency IMF2 as the dividing point, the wind power which the lithium battery and the supercapacitor undertake can be obtained respectively, we take region one as the example and the specific results are shown in Figures 7 and 8 below:

3.2 Power and Charge State Correction of the Hybrid Energy Storage Devices

However, the above power has not considered the power and charge state of the energy storage devices, so the fuzzy control algorithm is used to regulate the HESS. The membership functions can be seen in Figure 9 below.

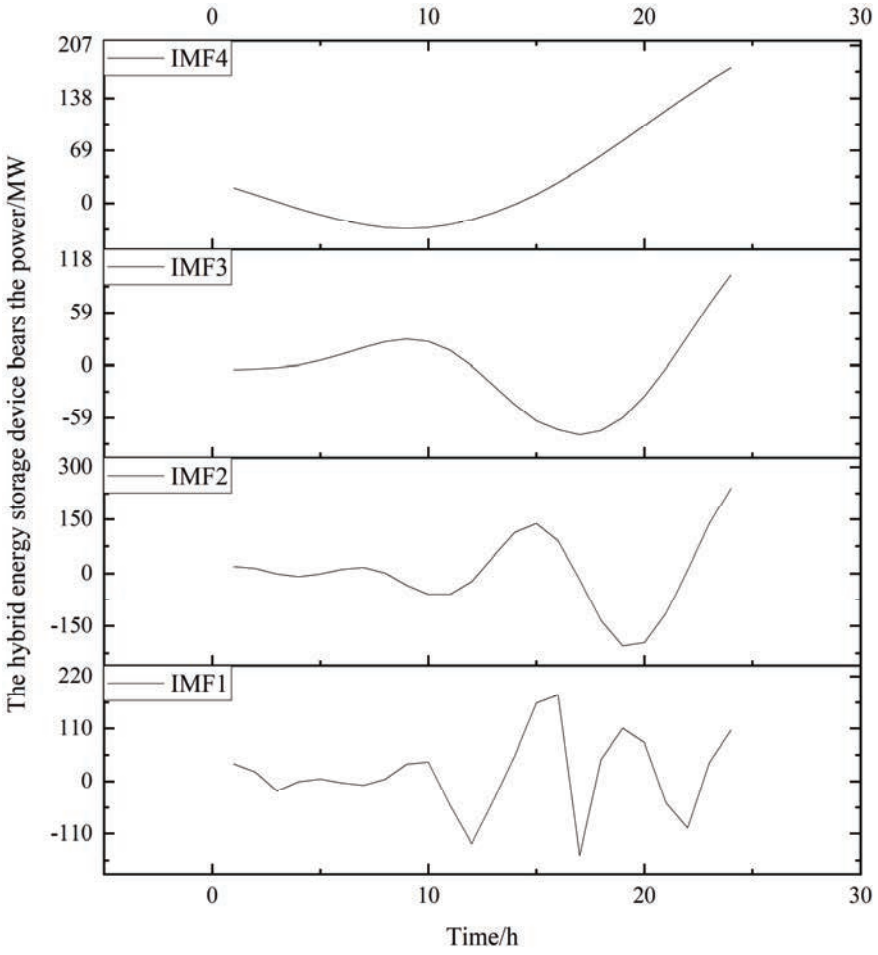

Figure 6 The frequency division diagram of the power decomposition signal assumed by the hybrid energy storage devices.

In addition to establishing the corresponding membership function for the input and output values, it is also necessary to establish the corresponding fuzzy control rule table according to different energy storage characteristics of the devices in the HESS. In this way, the HESS can be regulated more accurately, the power and charging state of the devices in the HESS can be maintained within a reasonable range of values.

According to the above membership functions, weighted average method (gravity center method) is used to clarify the fuzzy set of the output, and the

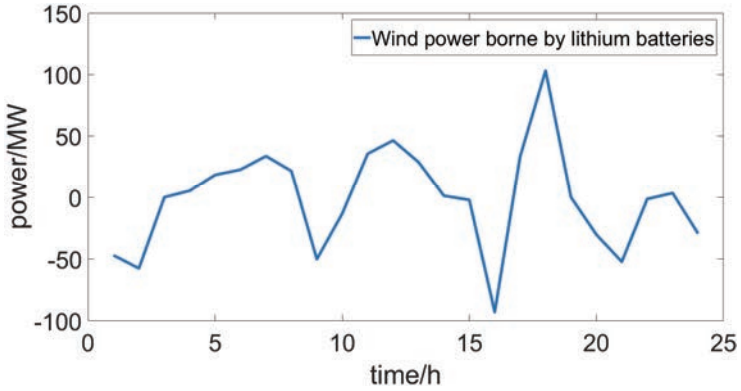

Figure 7 Region one lithium battery power diagram.

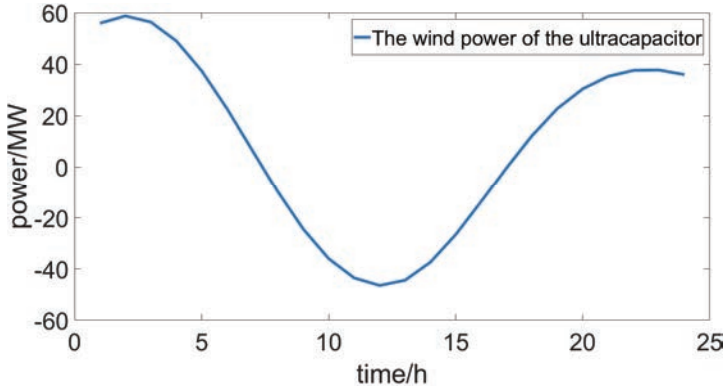

Figure 8 Region one supercapacitor power diagram.

real-time power correction coefficient can be obtained as follow:

$$k_x(t) = \frac{\sum_i \sum_j \mu_{\varepsilon_x(t),i} \mu_{\eta_x(t),j} \Delta k_x(t)}{\sum_i \sum_j \mu_{\varepsilon_x} \mu_{\eta_x(t),j}} \tag{30}$$

In formula (30): i and j can be NB, NS, ZO, PS, PB, and $\mu_{\varepsilon_x(t),i}$ and $\mu_{\eta_x(t),j}$ represent the corresponding membership values of the input $\varepsilon_x(t)$ and $\eta_x(t)$ respectively.

After obtaining the correction factor, the initial correction value of the devices power can be obtained as follow:

$$\Delta P_x(t) = \begin{cases} k_x(t)\ \widehat{P}_x^{+} & \widehat{P}_x^{+} \geq 0 \\ k_x(t)\ \widehat{P}_x^{-} & \widehat{P}_x^{-} < 0 \end{cases} \tag{31}$$

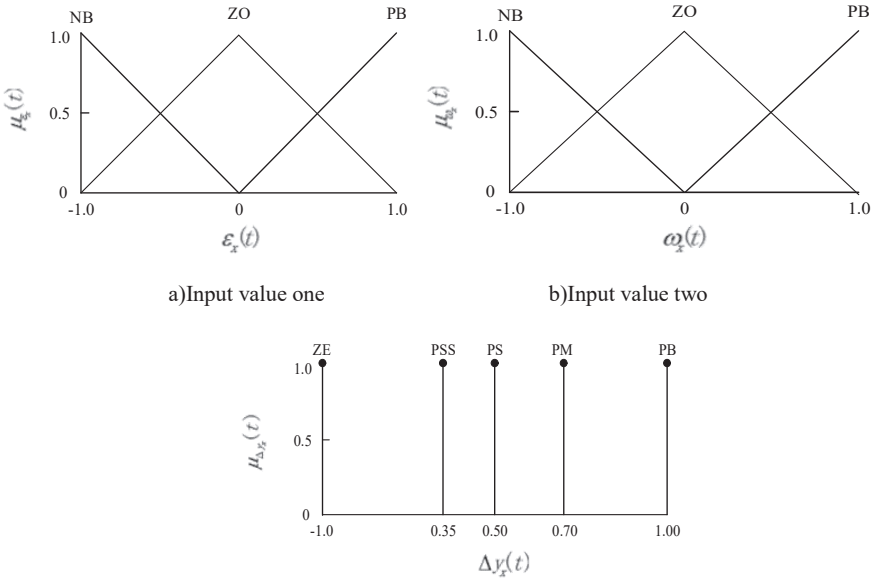

a)Input value one

b)Input value two

c)Output value

Figure 9 Input and output value membership function diagram.

And Figure 10 shows the SOC states of the lithium battery and the supercapacitor which are optimized by the fuzzy control algorithm:

According to the above results, it can be seen that the combination of the convolutional filtering algorithm, the ICEEMDAN algorithm and the fuzzy control algorithm can develop the charging and discharging strategy of the HESS better. Besides, the phenomenon of the overcharge and overdischarge does not occur in the HESS, the states of charge (SOC value) matain in (0.2, 0.8), and the overall action strategy is also good, which can give full play to the synergy of the HESS in the IES.

4 Collaborative Optimization Strategy

4.1 Collaborative Optimization Model of the MRIES

In this section, the entire MRIES is modeled. And the MRIES has the characteristics that a variety of heterogeneous energies are couplied and many equipments are involved in the energy exchange. Considering the operation characteristics of the equipments in the MRIES, combined with the actual

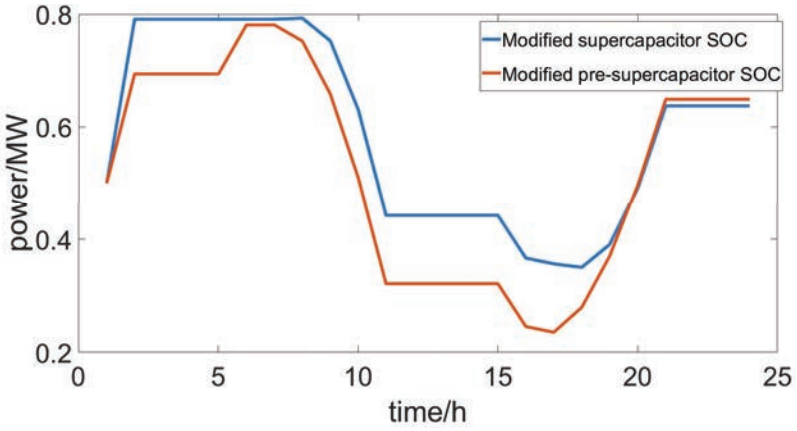

a) Region one Comparison of the ultracapacitor SOC before and after correction

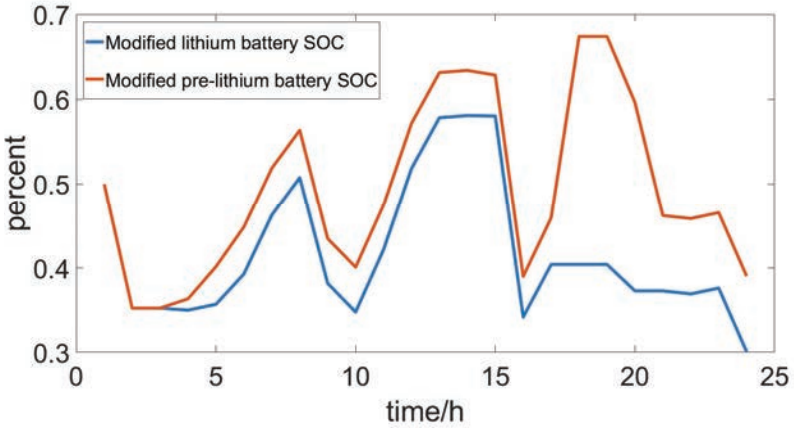

b) Region one Comparison of lithium battery SOC before and after correction

Figure 10 Region one SOC comparison diagram of the hybrid energy storage devices before and after correction.

production requirements, the objective function of the MRIES is established, which is composed of the energy cost, the carbon emission and the renewable energy utilization rate. And the objective functions consists of two parts, one is the internal objective function of each regional IES, and the other is the overall objective function of the MRIES.

The internal objective functions of the IES in each region are as follows:

$$MinF = (F_1, F_2, -F_3) \tag{32}$$

$$F_1 = \sum_{t=1}^{T} |K_{m,t} * P_{m,t}| \tag{33}$$

$$F_2 = \sum_{t=1}^{T} C_{gas,co_2} * P_{gas,t}^{m} + \sum_{t=1}^{T} C_{grid,co_2} * P_{grid,t}^{m} \tag{34}$$

$$F_3 = \sum_{t=1}^{T} (P_{wind,t} + P_{solar,t}) \Big/ \sum_{t=1}^{T} (P_{wind,t}^{theory} + P_{solar,t}^{theory}) \tag{35}$$

In formula (32), F_1 represents the energy cost, F_2 represents the carbon emission, and F_3 represents the renewable energy utilization rate in each region. In formula (33), $P_{m,t}$ and $K_{m,t}$ represent the power output value and the energy consumption price of different units respectively. The unit price of the gas turbine is 2.5, the unit price of the gas-fired boiler is 2.2, and the unit price of the fuel cell is 1.8. Besides, the electricity price refers to the TOU electric price mentioned in Chapter 2. In formula (34), $P_{gas,t}^{m}$ and C_{gas,co_2} represent the power output value of each gas-consuming unit and the amount of CO_2 production per unit of the gas-consuming power, which is 0.62 in this paper, $P_{grid,t}^{m}$ and C_{grid,co_2} represent the electric power which is from the power grid and the amount of CO_2 production per unit of the power-purchasing power respectively, which is 1.15 in this paper, In formula (35), $P_{wind,t}$ 和 $P_{solar,t}$ represent the wind power and the photovoltaic power respectively which are consumed in the IES of each region, $P_{wind,t}^{theory}$ and $P_{solar,t}^{theory}$ represent the total wind and photovoltaic power in the IES of each region.

Combined with the above each regional IES objective functions, the overall objective functions of the entire MRIES are as follows:

$$MinMG = (MG_1, MG_2, MG_3) \tag{36}$$

$$MG_1 = w_1 * F_1^{one} + w_2 * F_2^{one} - w_3 * F_3^{one} \tag{37}$$

$$MG_2 = w_1 * F_1^{two} + w_2 * F_2^{two} - w_3 * F_3^{two} \tag{38}$$

$$MG_3 = w_1 * F_1^{three} + w_2 * F_2^{three} - w_3 * F_3^{three} \tag{39}$$

In formula (36), MG_1, MG_2 and MG_3 represent the objective functions of the energy networks in the three IESs respectively, In formula (37), (38) and (39), w_1, w_2, w_3 represent the weight values of the three evaluation indexes in each regional IES respectively. F_1^{one}, F_2^{one}, F_3^{one} represent the energy cost, the carbon emission and the renewable energy utilization rate in the region one IES. And so on as F_1^{two}, F_2^{two}, F_3^{two} and F_1^{three}, F_2^{three}, F_3^{three}. Since the three evaluation indexes are regarded as equally important in this paper, w_1, w_2, w_3 can be obtained by the analytic hierarchy process and they are all 1/3.

4.2 BWO Algorithm

The BWO algorithm is inspired by the daily life behaviors of the beluga whales. Beluga whales are known for their unique pure white appearance and color, and they are highly social mammals. They live in groups generally, with 2 to 25 members in a group, and the number of group members is generally around 10. Similar to other meta-heuristic optimization algorithms, the BWO algorithm includes an exploration phase which is established by considering the beluga whales' swimming behaviors and a development phase which is inspired by the beluga whale predation behaviors, as well as the whale drop phenomenon that exists in the nature.

5 Results and Discussion

In the optimization process of the MRIES, we should not only consider the load power distribution and optimization of each regional IES, but also consider the energy exchange among three IESs. Therefore, in addition to the optimization results of the whole MRIES, we also need to conduct in-depth studies for each region separately. Considering the uncertainty of the optimization results, an optimization result with the best effect among multiple optimization results is selected for the presentation. Besides, the optimized power distribution results of the electric, hot and cold loads before and after the algorithm improvement are compared. This chapter also compares the optimization results of the energy cost, the carbon emission and the renewable energy utilization rate of the whole MRIES before and after the algorithm improvement. The optimization results of using different optimization algorithms as the collaborative optimization strategies for the MRIESs are shown below.

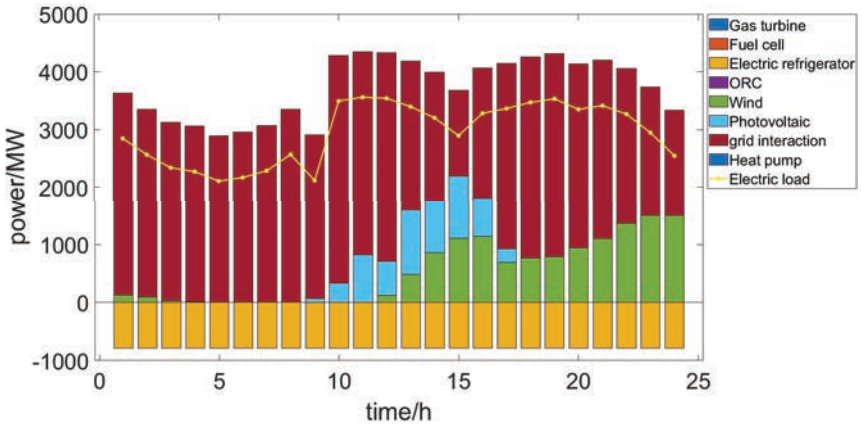

Figure 11 Region three electric load power balance diagram optimized by the BWO algorithm.

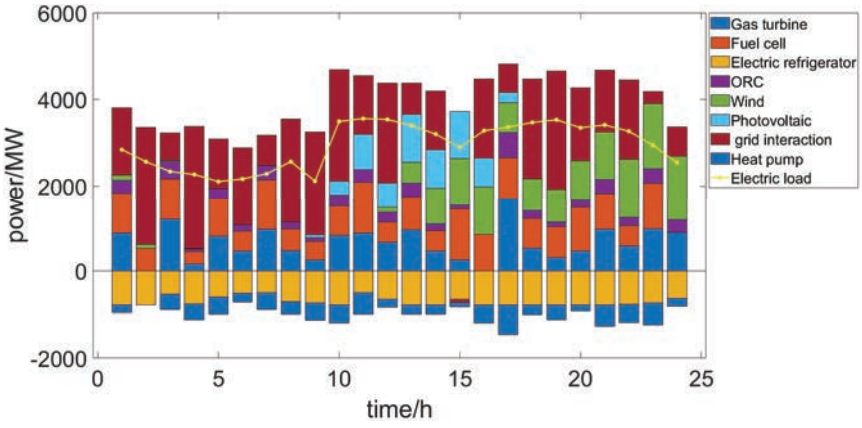

Figure 12 Region three electric load power balance diagram optimized by the IBWO algorithm.

5.1 Comparison of the Collaborative Optimization Results of Each Region Between the BWO and the IBWO Algorithm

Taking the optimization results of the region three IES as the example, the optimization ability of the BWO and IBWO algorithm can be felt more intuitively by comparing the optimization results. The power balance optimization results of the cold, hot and electric loads in the region three IES

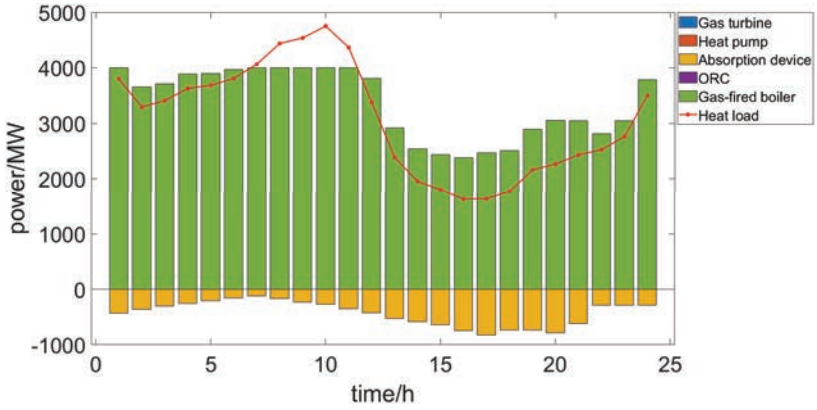

Figure 13 Region three thermal load power balance diagram optimized by the BWO algorithm.

before and after the algorithm improvement are shown in Figures 11 to 16 below:

As shown in Figure 11, it is obvious that the optimization results of the BWO algorithm only include four kinds of the power supply and loss components, including the power supply of the renewable energy, the interactive power of the energy networks and the power loss of the electric refrigerator, which is obviously unreasonable extremely. In Figure 12, the result after the IBWO algorithm optimization include the gas turbine power supply, the fuel cell power supply, the electric refrigerator power loss, the ORC power generation power supply, the renewable energy power supply, the energy networks interaction power supply and the thermal pump power loss. Compared with the optimization result in Figure 11, the equipments that participate in the power supply and loss is more diverse, which make full use of various equipments in the region three IES, avoiding the waste of the resources.

As can be seen in Figure 13, in the optimization results of the region three thermal power with the BWO algorithm, only the gas boiler and the absorption device exist, and the total thermal power in the region three IES fails to meet the demand of its thermal load from 7 o 'clock to 11 o 'clock. Therefore, the region three IES needs to buy electricity from the grid and then converts it into the thermal power to meet its thermal load demand, obviously this will greatly increase the energy cost of the region three IES, resulting in huge energy waste, which is undesirable. In contrast, as shown in Figure 14, in the optimization results of the IBWO algorithm, not only do all devices

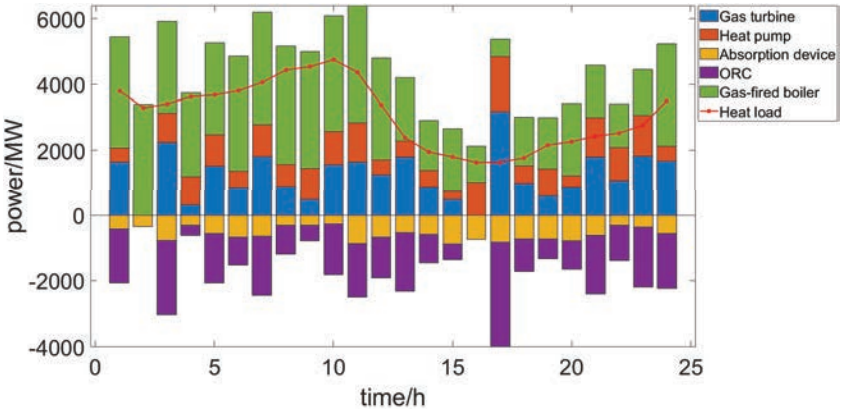

Figure 14 Region three hot load power balance diagram optimized by the IBWO algorithm.

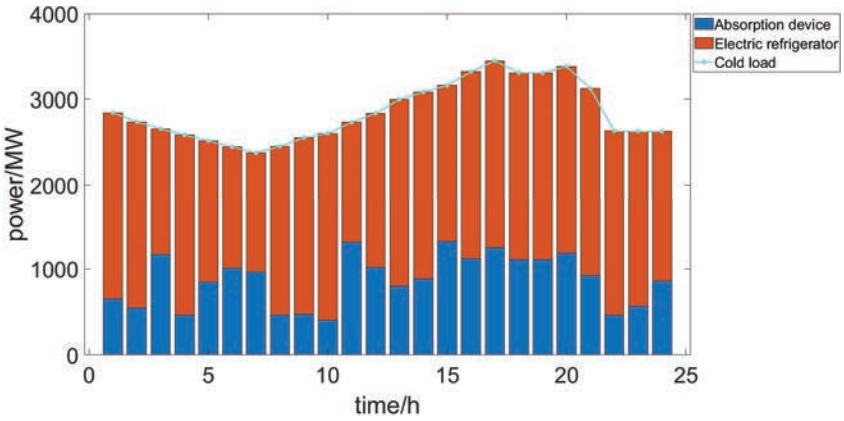

Figure 15 Region three cold load power balance diagram optimized by the original algorithm.

participate in the power balance of the thermal load, but the IBWO algorithm also ensures that the power requirment of the thermal load can be satisfied within 24 hours all day.

As shown in Figures 15 and 16, in the region three IES, since the cold load power demand is only provided by the absorption devices and the electric refrigerators, both refrigeration equipments participate in the cold load supply in the region three IES, ensuring the balance of the cold load supply in the final optimization result.

All results above show that the BWO algorithm does not show a good optimization effect when dealing with the power balances of the electric

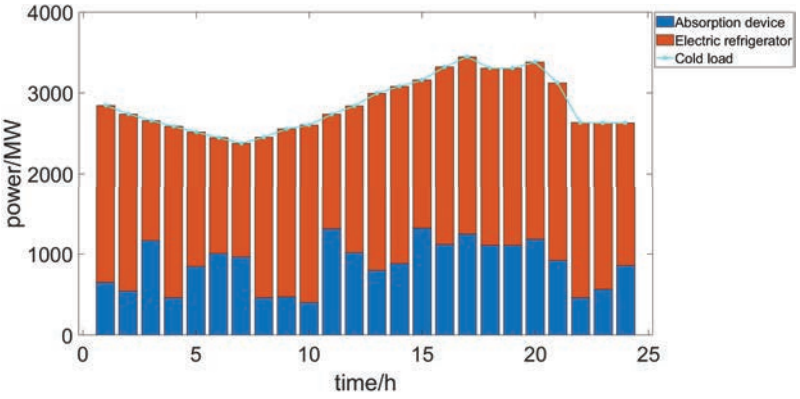

Figure 16 Region three cold load power balance diagram optimized by the improved algorithm.

load and the thermal load in the region three IES. In contrast, the IBWO algorithm shows a better optimization effect in the power distribution with various equipments. Not only all the corresponding equipments participate in the energy power balances of the electricic and thermal load, but also meet the power requirments of the electricic and thermal load in the region three IES.

5.2 Comparison of the Overall System Results Between the BWO and the IBWO Algorithm

In addition to the above optimization results of the power distribution which need to meet the cold, hot and electric loads in region three, this section also considers three indexes of the energy cost, the carbon emission and the renewable energy utilization rate as the evaluation indexes of the system optimization effect. Finally, the fitness value of the system which is optimized by the algorithm can be obtained after linear addition of the three indexes above, and that is, the total cost of the entire MRIES. By comparing the optimization results of the BWO and IBWO algorithm, the superiority of the IBWO algorithm can be more understood intuitively.

The BWO and IBWO algorithm fitness values are shown in Figure 17 below:

As shown in Figure 17, the IBWO algorithm fitness value is far lower than the BWO algorithm fitness value, which means that the IBWO algorithm performs better than the BWO algorithm in the MRIES.

As can be seen in Table 1, although the IBWO algorithm optimization has no significant promotion in the index of the iterations and the time, the total

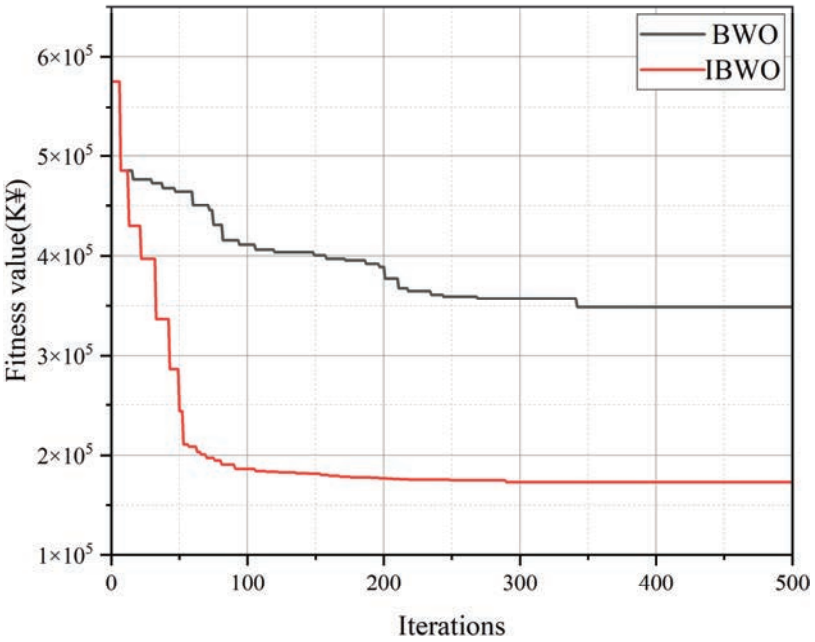

Figure 17 Comparison of the BWO and IBWO algorithm fitness values.

Table 1 Comparison of the BWO and IBWO algorithm optimization results

Name	Iterations	Cost	Time
BWO	339	348733.4141	81
IBWO	281	173435.7392	63

Table 2 Comparison 2 of the BWO and IBWO optimization results

Name	Energy cost	Carbon emission	Utilization rate
BWO	154362.3711	194371.0430	100%
IBWO	91357.5263	82078.2099	100%

cost is reduced by about half, which saves great cost for the entire MRIES. Through the collaborative optimization strategy of the MRIES, the total cost of the whole MRIES is greatly reduced.

As shown in Table 2, the optimization result with the IBWO algorithm are much better than that with the BWO algorithm, and the equipments which particpate in the power supply of the electricity and thermal load are too single in the BWO optimization result, it will lead to the reduction of the energy efficiency in the entire MRIES, which will not only lead to the

increase of the energy cost, but also greatly increase its carbon emission. And the collaborative optimization strategy which is based on the IBWO algorithm can greatly reduce the total cost of the whole MRIES. In the results of the two algorithms optimization, the renewable energy utilization rates are both 100%, because the MRIES gives priority to the renewable energy consumption and the renewable energy power is fully utilized.

6 Conclusion

The MRIES is taken as the research object, including electricity, thermal, cold, gas and the storage. After considering the renewable energy uncertainty, the collaborative optimization strategy of the MRIES based on multiple models and constraints is studied. The main research results are as follows:

(1) Aiming at the uncertainty of the wind power in the IES, a hybrid energy storage solution strategy is proposed. Firstly, the convolutional filtering algorithm is used to smooth the data. And the power difference of the wind power data before and after smoothing is taken as the power which is borne by the HESS, and it is also used as the input data of the ICEEMDAN algorithm to obtain the decomposed wind power data, and then the decomposed data is divided into two kinds of the frequency components, in which the high one is borne by the supercapacitor and the low one is borne by the lithium battery. And the fuzzy control algorithm is used to regulate the HESS. The optimization results show that with the help of the convolutional filtering algorithm, the ICEEMDAN algorithm and the fuzzy control algorithm, we can better develop the charging and discharging strategy of the HESS. Besides, the phenomenon of the overcharge and overdischarge does not occur in the HESS, the states of charge (SOC value) matain in (0.2,0.8), and the overall action strategy is also good, which can give full play to the synergy of the HESS in the IES.

(2) To realize the collaborative optimization of the MRIES, the IBWO algorithm is proposed, which takes the energy cost, the carbon emission and the renewable energy utilization rate as the optimization objectives of the IES. The collaborative optimization scheme ensures the stability of the whole MRIES, and realizes the optimization reasonly.

Although this paper has made some achievements in the research of MRIES, there are still many shortcomings. In the future, further research on the IES can be considered from the following aspects:

(1) As the system control performance requirements become higher and higher, most of the current research is carried out from the scheduling aspect, although this paper studies the IES from the modeling aspect, but the modeling of each energy subsystem is not enough. In the future, more in-depth research on modeling can be considered.
(2) This paper deals with the uncertainty of the wind power mainly, and does not deal with the photovoltaic power generation specifically. In the future, different targeted treatments can be considered for the corresponding renewable energies which have different characteristics to solve the access problem of the renewable energy better.
(3) An integrated demand response model based on the TOU electricity price mechanism is established on the load side, which is not enough obviously to mobilize the reducible load demand of the users fully. In the future, more integrated demand response methods need to be considered to regulate the load.
(4) The collaborative optimization strategy which is adopted in this paper only uses the IBWO algorithm, which has a good effect. In the future, more optimization methods can be considered to participate in the collaborative optimization of the MRIES, so as to increase the diversity of the strategies and achieve better collaborative optimization effects.

References

[1] Atinkut B., Degarege A., Baseem K., et al. Grid Integration of Hybrid Energy System for Distribution Network[J]. Distributed Generation & Alternative Energy Journal, 2022, 37(3): 537–556.
[2] Guo H., Ren Y., Zhao Q., et al. Techno-economic Analysis of Renewable-based Stand-alone Hybrid Energy Systems Considering Load Growth and Photovoltaic Depreciation Rates[J]. Distributed Generation & Alternative Energy Journal, 2020, 35(3): 209–236.
[3] Tan J., Wu Q., Hu Q., et al. Adaptive robust energy and reserve co-optimization of integrated electricity and thermaling system considering wind uncertainty[J]. Applied Energy, 2020, 260: 114230. https://doi.org/10.1016/j.apenergy.2019.114230.
[4] Duan J, Yang Y, Liu F, et al. Distributed optimization of integrated electricity-natural gas distribution networks considering wind power uncertainties[J]. International Journal of Electrical Power & Energy Systems, 2022, 135: 107460. https://doi.org/10.1016/j.ijepes.2021.107460.

[5] Lu N, Su C, Guo C, et al. Stochastic optimal scheduling of wind power and pumped-storage hydropower complementary systems with multiple uncertainties[J]. Journal of Energy Storage, 2024, 78: 110060. https://doi.org/10.1016/j.est.2023.110060.

[6] Liu X., LIU J., Yang Y., et al. Uncertainty collaborative planning method of integrated energy system considering low-carbon transformation of multi-function zone and multi-mode utilization of low-carbon characteristics of hydrogen energy [J/OL]. Power grid technology, 2024: 1–17. https://doi.org/10.13335/j.1000-3673.pst.2023.2054.

[7] Wang L., Hou C., Ye B., et al. Optimal Operation Analysis of Integrated Community Energy System Considering the Uncertainty of Demand Response[J]. IEEE Transactions on Power Systems[J]. 2021, 36(4): 3681-3691. https://doi:10.1109/TPWRS.2021.3051720.

[8] Zhang Z., Wang C., Wu Q., et al. Optimal dispatch for cross-regional integrated energy system with renewable energy uncertainties: A unified spatial-temporal cooperative framework[J]. Energy, 2024, 292: 130433. https://doi.org/10.1016/j.energy.2024.130433.

[9] Mu Y., Wang C., Cao Y., et al. A CVaR-based risk assessment method for park-level integrated energy system considering the uncertainties and correlation of energy prices[J]. Energy, 2022, 247: 123549. https://doi.org/10.1016/j.energy.2022.123549.

[10] Fahim M., Anwar A., Shoaib A., et al. Hybrid Energy System Modelling for Oil & Gas Fields: A Case Study of Pasakhi Satellite Oil & Gas Complex[J]. Distributed Generation & Alternative Energy Journal, 2022, 37(2): 281–310.

[11] Shang W, LI G, Ding Y, et al. A collaborative scheduling method for integrated energy system considering the uncertainty of source load and new energy consumption[J]. Power grid technology, 2024, 48(02): 517–532. https://doi:10.13335/j.1000-3673.pst.2023.0577.

[12] Li P, Wang J, Li C, et al. A collaborative optimization operation method of integrated energy system in Park considering the uncertainty of source load and the characteristics of equipment operating conditions [J]. Proceedings of the CSEE, 2023, 43(20): 7802–7812. https://doi:10.13334/j.0258-8013.pcsee.222753.

[13] Li Y., Han M., Han Z., et al. Coordinating Flexible Demand Response and Renewable Uncertainties for Scheduling of Community Integrated Energy Systems With an Electric Vehicle Charging Station: A Bi-Level Approach[J]. IEEE Transactions on Sustainable Energy, 2021, 12(4): 2321–2331. https://doi:10.1109/TSTE.2021.3090463.

[14] Dong Y., Zhang H., Ma P., et al. A hybrid robust-interval optimization approach for integrated energy systems planning under uncertainties[J]. Energy, 2023, 274: 127267. https://doi.org/10.1016/j.energy.2023.127267.

[15] Lin J., Gao C., Zeng J., et al. Stackelberg-Nash asymmetric bargaining-based scheduling optimization and revenue-allocation for multi-operator regional integrated energy system considering competition-cooperation relationship and source-load uncertainties[J]. Energy, 2024, 291: 130262. https://doi.org/10.1016/j.energy.2024.130262.

[16] Wang Y., Zheng Y., Yang Q., et al. Day-ahead bidding strategy of regional integrated energy systems considering multiple uncertainties in electricity markets[J]. Applied Energy, 2023, 348: 121511. https://doi.org/10.1016/j.apenergy.2023.121511.

[17] Liu Z., Cui Y., Wang J., et al. Multi-objective optimization of multi-energy complementary integrated energy systems considering load prediction and renewable energy production uncertainties[J]. Energy, 2022, 254: 124399. https://doi.org/10.1016/j.energy.2022.124399.

[18] Zhou G., Bai M., Li H., et al. Multi-objective station-network synergy planning for regional integrated energy system considering energy cascade utilization and uncertainty[J]. Energy Conversion and Management, 2024, 301: 118073. https://doi.org/10.1016/j.enconman.2024.118073.

[19] Huang S., Lu H., Chen M., et al. Integrated energy system scheduling considering the correlation of uncertainties[J]. Energy, 2023, 283: 129011. https://doi.org/10.1016/j.energy.2023.129011.

[20] Zhou Y., Ma Z., Shi X., et al. Multi-agent optimal scheduling for integrated energy system considering the global carbon emission constraint[J]. Energy, 2024, 288: 129732. https://doi.org/10.1016/j.energy.2023.129732.

[21] Wang Q., Wang Y., Chen Z., et al. Multi-agent system consistency-based cooperative scheduling strategy of regional integrated energy system[J]. Energy, 2024, 295: 130904. https://doi.org/10.1016/j.energy.2024.130904.

[22] Liu J., Li Y., Ma Y., et al. Coordinated energy management for integrated energy system incorporating multiple flexibility measures of supply and demand sides: A deep reinforcement learning approach[J]. Energy Conversion and Management, 2023, 297: 117728. https://doi.org/10.1016/j.enconman.2023.117728.

[23] Li K., Ye N., Li S., et al. Distributed collaborative operation strategies in multi-agent integrated energy system considering integrated demand response based on game theory[J]. Energy, 2023, 273: 127137. https://doi.org/10.1016/j.energy.2023.127137.

[24] Liang Z., Mu L. Multi-agent low-carbon optimal dispatch of regional integrated energy system based on mixed game theory[J]. Energy, 2024, 295: 130953. https://doi.org/10.1016/j.energy.2024.130953.

[25] Li Z., Xia Y, Bo Y., et al. Optimal planning for electricity-hydrogen integrated energy system considering multiple timescale operations and representative time-period selection[J]. Applied Energy, 2024, 362: 122965. https://doi.org/10.1016/j.apenergy.2024.122965.

[26] Liu S., Song L., Wang T., et al. Negative carbon optimal scheduling of integrated energy system using a non-dominant sorting genetic algorithm[J]. Energy Conversion and Management, 2023, 291: 117345. https://doi.org/10.1016/j.enconman.2023.117345.

[27] Pan C., Fan H., Zhang R., et al. An improved multi-timescale coordinated control strategy for an integrated energy system with a hybrid energy storage system[J]. Applied Energy, 2023, 343: 121137. https://doi.org/10.1016/j.apenergy.2023.121137.

[28] Xu Z., Han G., Han L., et al. Multi-Energy Scheduling of an Industrial Integrated Energy System by Reinforcement Learning-Based Differential Evolution[J]. IEEE Transactions on Green Communications and Networking, 2021, 5(3): 1077–1090. https://doi:10.1109/TGCN.2021.3061789.

[29] Guo J., Wu D., Wang Y., et al. Co-optimization method research and comprehensive benefits analysis of regional integrated energy system[J]. Applied Energy, 2023, 340: 121034. https://doi.org/10.1016/j.apenergy.2023.121034.

[30] Yang W., Huang Y., Huang T., et al. Hybrid continuous-discrete time control strategy to optimize thermal network dynamic storage and thermal-electricity integrated energy system dynamic operation[J]. Energy Conversion and Management, 2024, 301: 118035.

[31] Wang X., Han Li., Wang C., et al. A time-scale adaptive dispatching strategy considering the matching of time characteristics and dispatching periods of the integrated energy system[J]. Energy, 2023, 267: 126584. https://doi.org/10.1016/j.energy.2022.126584.

[32] Ma X., Peng B., Ma X., et al. Multi-timescale optimization scheduling of regional integrated energy system based on source-load joint

forecasting[J]. Energy, 2023, 283: 129186. https://doi.org/10.1016/j.energy.2023.129186.

[33] Wang L., Lin J., Dong H., et al. Demand response comprehensive incentive mechanism-based multi-time scale optimization scheduling for park integrated energy system[J]. Energy, 2023, 270: 126893. https://doi.org/10.1016/j.energy.2023.126893.

[34] Cai P., Mi Y., Ma S., et al. Hierarchical game for integrated energy system and electricity-hydrogen hybrid charging station under distributionally robust optimization[J]. Energy, 2023, 283: 128471. https://doi.org/10.1016/j.energy.2023.128471.

[35] Zhang Z., Wang C., Wu Q., et al. Optimal dispatch for cross-regional integrated energy system with renewable energy uncertainties: A unified spatial-temporal cooperative framework[J]. Energy, 2024, 292: 130433. https://doi.org/10.1016/j.energy.2024.130433.

[36] Liu J., Li Yao., Ma Y., et al. Two-layer multiple scenario optimization framework for integrated energy system based on optimal energy contribution ratio strategy[J]. Energy, 2023, 285: 128673. https://doi.org/10.1016/j.energy.2023.128673.

[37] Yang X., Zhang Z., Mei L., et al. Optimal configuration of improved integrated energy system based on stepped carbon penalty response and improved power to gas[J]. Energy, 2023, 263: 125985. https://doi.org/10.1016/j.energy.2022.125985.

[38] Duan P., Zhao B., Zhang X., et al. A day-ahead optimal operation strategy for integrated energy systems in multi-public buildings based on cooperative game[J]. Energy, 2023, 275: 127395. https://doi.org/10.1016/j.energy.2023.127395.

[39] Zheng L., Wu H., Guo S., et al. Real-time dispatch of an integrated energy system based on multi-stage reinforcement learning with an improved action-choosing strategy[J]. Energy, 2023, 277: 127636. https://doi.org/10.1016/j.energy.2023.127636.

Biography

Ming Liu, the student of the School of Control and Computer Engineering, North China Electric Power University.

Specialty: Control science and engineering.

Research direction: Integrated energy system.